Heliyon 8 (2022) e08689

Contents lists available at ScienceDirect

Heliyon

journal homepage: www.cell.com/heliyon

Research article

Presence of activated carbon particles from waste walnut shell as a biosorbent in monoethanolamine (MEA) solution to enhance carbon dioxide absorption

Zohreh Khoshraftar, Ahad Ghaemi *

School of Chemical, Petroleum and Gas Engineering, Iran University of Science and Technology, P.O. Box: 16765-163, Tehran, Iran

ARTICLE INFO

Keywords:
Carbon dioxide
Absorption
Monoethanolamine
Activated carbon
Biosorbent

ABSTRACT

Greenhouse effects are a natural phenomenon that plays a high role in shaping the climate system. In this research, MEA solution was used for CO_2 capture in presence of activated carbon particles from waste walnut shells as a biosorbent. The process parameters including temperature, pressure, MEA concentration, and activated carbon were used in the central composite design (CCD) model. The absorption experiments were carried out in a laboratory setup at operational conditions including temperature in range of 20–60 °C, pressure in range of 3.5–9.5 bar, MEA concentration in range of 2.5–8.5 wt%, and active carbon amount in range of 0.3–0.9 g/L. The process responses including CO_2 loading, the amounts of CO_2 absorption, and absorption percentage were obtained in the range of 0.444–0.720 mol_{CO2}/mol_{MEA}, 0.294–0.687 mol/L, and 19.32–52.25%, respectively. The optimal value of CO_2 loading was obtained at temperature of 30 °C, pressure of 5.19 bar, activated carbon of 0.75 g, and MEA concentration of 7.00 wt%. The optimum values of responses were obtained 0.531, 0.609 mol/L and 50.04% for maximum loading, absorption amount, and absorption percentage, respectively. From the results, carbon dioxide loading in MEA solution increases in presence of activated carbon particles.

1. Introduction

Greenhouse effects are a natural phenomenon that plays a high role in shaping the climate system (Penchah et al., 2021; Wang et al., 2017). This phenomenon provides relative warmth and a favorable environment near the surface earth, where humans and other living organisms can grow and develop (Khajeh and Ghaemi, 2021; Shao et al., 2019). It is one of the vast biological, chemical, and physical processes involved in determining the climate. The relationship between increasing greenhouse effects and global climate change is not an easy one. Not only does it increase the concentration of greenhouse gases in the atmosphere, but it also increases the concentration of pollutants in the oceans, soil, and biosphere (Behroozi et al., 2021; Monastersky, 2013; Shao et al., 2019). There is a natural greenhouse effect whose effects remain before human activities, and it is a greenhouse effect resulting from human activities (Wang et al., 2017). Therefore, when we release excess carbon dioxide or methane or nitrous oxide into the atmosphere, all the molecules we add work like little heating machines. The global temperature is forecast to rise, resulting in a 59 cm rise in sea level (Amiri et al., 2017; Pashaei et al., 2017; Ran et al., 2017; Saeidi et al., 2018). The most important subject that has attracted many scientists' attention today is global warming due to greenhouse gases, which has put the world on the brink of a large human and environmental catastrophe. In addition, scientists believe that the most critical cause of the combustion of fossil fuels is the release of carbon dioxide and mineral fuels in industrialized countries (Naeem et al., 2016; Wu et al., 2020). Carbon dioxide is produced from burning organic matter in the presence of sufficient oxygen. Plants use carbon dioxide in the photosynthesis process to make carbohydrates, and by absorbing it, they release oxygen (Shahbazi and Nasab, 2016). If irreversible harm to the climate system has been avoided, the development of appropriate control strategies and cost-effective technologies to minimize CO_2 emissions is necessary (Karami and Ghaemi, 2021). The CO_2 emissions should reduce as soon as possible. CCS (carbon capture and storage) is a viable technology for addressing this issue (Mirzaei and Ghaemi, 2020; Ran et al., 2017). There are several ways to separate and remove CO_2. The most important processes are adsorption, absorption, membrane separation, and cryogenic distillation. It is more appropriate to use absorption among these methods (Rinprasertmeechai et al., 2012; Wang et al., 2014). In the adsorption process, a solid adsorbent is applied to absorb CO_2 on its surface. Surface area, selectivity, and high

* Corresponding author.
E-mail address: aghaemi@iust.ac.ir (A. Ghaemi).

https://doi.org/10.1016/j.heliyon.2021.e08689
Received 19 October 2021; Received in revised form 17 November 2021; Accepted 24 December 2021

recoverability are significant indicators in selecting adsorbents (Leung et al., 2014). One of the significant issues in the absorption process is choosing the right solvent. Since the absorption process is economically highly dependent on the selected solvent, it is significant to conduct studies to take the best solvent (Aschenbrenner and Styring, 2010). Carbonaceous adsorbents in comparison to zeolites, calcium oxides, hydrotalcite, and metal-organic frameworks (MOFs) have demonstrated several advantages (González and Manyà, 2020). They are more resistant to moisture and have greater thermal, mechanical, and chemical stability while requiring less energy (Yang et al., 2016). Further, using waste biomass as a precursor to producing these sorbents will increase its attractiveness as an effective CO_2 capture method because of their relative simplicity to synthesize and low cost of production (Gao et al., 2016; González and Manyà, 2020). Chemical absorption with an amine solution is the traditional method for CO_2 capture (Shao et al., 2019; Songolzadeh et al., 2014). Amines are selectable, reversible, relatively non-volatile, inexpensive, and highly reactive. The most common Alkanolamine used in CO_2 removal includes monoethanolamine (MEA), diethanolamine (DEA), methyl ethanolamine (MMEA), methyl diethanolamine (MDEA), aminomethyl propanol (AMP), diethylene glycol amine (DGA), diisopropanolamine (DIPA), piperazine (PZ), and triethanolamine (TEA) (Karnwiboon et al., 2017). Monoethanolamine is one of the most common amines that has been used for years to absorb carbon dioxide and hydrogen sulfide from natural gases. Monoethanolamine is applied as an aqueous solution with a concentration of 10–20% by weight. Because monoethanolamine is one of the primary types of amines, it forms stronger bonds with carbon dioxide (Gupta et al., 2003). Although the absorption process with aqueous solutions effectively removes CO_2, it has many economic and environmental problems, including high energy costs for solvent reduction, solvent loss due to evaporation, thermal degradability, and corrosion instruments equipment during the process (Karbalaei Mohammad et al., 2020). The MEA solution has one of the greatest advantages over other amines in terms of the rate at which it reacts with CO_2 because of the formation of carbamate, which allows a packed column to have a smaller height and size (Ramezani et al., 2021). Adsorption of carbon dioxide with activated carbon based on amino solvents can solve the problems caused by amino solvents (Karbalaei Mohammad et al., 2020). In contrast to many studies on the solubility of acid gases in aqueous amine solutions, few experimental studies have reported on amino solvent systems in the presence of physical absorption. A summary the work done on chemical solvents and the use of solid particles in these solvents is summarized. Donaldson and Nguyen (1980) examined the reaction between tertiary amines and carbon dioxide and showed that the rate of absorption of tertiary amines was slower than that of primary and secondary types (Donaldson and Nguyen, 1980). Little et al. (1990) studied the reaction kinetics between carbon dioxide and TEA and DEMEA (diethyl monoethanolamine) amines. They reported linear relationships between the quadratic velocity constant and temperature (Littel et al., 1990). Wang et al. (2004) used membrane contactors to adsorb CO_2 into amine solutions. They used three common 2-amino-2-methyl-1-propanol (AMP), DEA, and MDEA amino alcohol solutions to evaluate the effect of different sorption processes, operating parameters, and membrane properties of CO_2 absorption behavior (Wang et al., 2004). In the recent years, the response surface methodology (RSM) has been considered an efficient technique to optimize and reduce the number of experiments. As a result, it has attracted the attention of many researchers, and it was designed using the RSM method based on central composite design (Ghaemi et al., 2021; Pashaei et al., 2020).

Today, the use of solid particles in micro and nano dimensions in various chemical solvents, including amines, has been studied and tested (Karami and Ghaemi, 2021). Although many researchers have studied CO_2 uptake in different chemical solvents separately, limited equilibrium data on CO_2 uptake in amino solutions in the presence of solid particles are presented in the literature. The solubility data of CO_2 on MEA amine solutions are presented in Table 1. No experimental data on loading and absorption rates of CO_2 by MEA as amine solvent in the sources contain walnut shell activated carbon adsorbents were not presented. Little is known about physical adsorbents in amine solution for CO_2 absorption.

In the present study, the performance of CO_2 absorption into aqueous MEA solution was investigated experimentally in presence of activated carbon particles from waste walnut shell. The effects of operating parameters including MEA concentration, activated carbon amount, temperature and pressure on CO_2 loading and uptake were investigated. In addition, RSM was used to obtain the optimal conditions of CO_2 absorption into MEA solution in presence of activated carbon.

2. Materials and methods

2.1. Materials

Monoethanolamine (MEA) was purchased from Merck Company (Germany) with a purity of over 99%. Solid particles were prepared from activated carbon of waste walnut shell with the specifications including mesh size of 200 μm, total specific surface area of 881.84 m^2/g, and average pore diameter of 1.6746 nm. After the preparation of samples, they were kept in closed containers to prevent contact with air. CO_2 was prepared from Mehrabad Gas Company (Tehran, Iran), with a purity of over 99%.

2.2. Synthesis and activation of carbon

Walnut-shell waste was collected from walnut trees in Anzali port of Iran and washed in distilled water before being dried at 110 °C for 24 h. A fine powder was obtained by crushing, grinding, and sieving it through a 200 μm sized sieve, then used as a precursor for the production of AC. In the physical activation, water vapor are passed over a precursor at high temperatures. The walnut shells were hydrothermally carbonized to a higher temperature at 200 °C for 4 h in a high-pressure Parr reactor (18 bar) (Model 4550, Parr Instrument Company, Moline, Illinois). During HTC process, the hydrochar generated by HTC is dried for 12 h at 80 °C, after which it is steam activated for 3 h at 600 °C. The reactor for steam activation (Heating rate: 40 °C min^{-1}) was made of quartz with nitrogen and steam flowing upwards (Beri et al., 2021). The experimental stages of the adsorbent preparation was presented in Figure 1.

Table 1. Studies on CO_2 solubility in MEA solutions.

Ref.	CO_2 Loading (mol_{CO2}/mol_{amin})	C_{MEA} (mol/L)	P (bar)	T (K)	Type of Amine
(Shen and Li, 1992)	0.306–0.646	5	8.20–1183.70	333, 353, 373	MEA
Jane and Li, 1997	0.215–0.473	2.400	8.68–121.8	353	MEA
J.-Y. Park et al., 2002	0.562–1.068	0.183, 0.278	13.1–2989.1	313	MEA
(S. H. Park et al., 2002)	0.575–0.683	0.531, 0.5333, 0.536	10.62–320.13	313, 333, 353	MEA
(Ma'mun et al., 2005)	0.176–0.418	0.525	9.045–191.9	393	MEA
(Gabrielsen et al., 2005)	0.215–0.473		9.87–398.7	353, 373, 393	MEA
(Khodadadi et al., 2019)	0.410–0.711 0.419–0.671 0.382–0.618	-	0.1324–1.2617 0.1779–1.6065 0.2406–1.2714	313, 323, 333	MEA + DAP

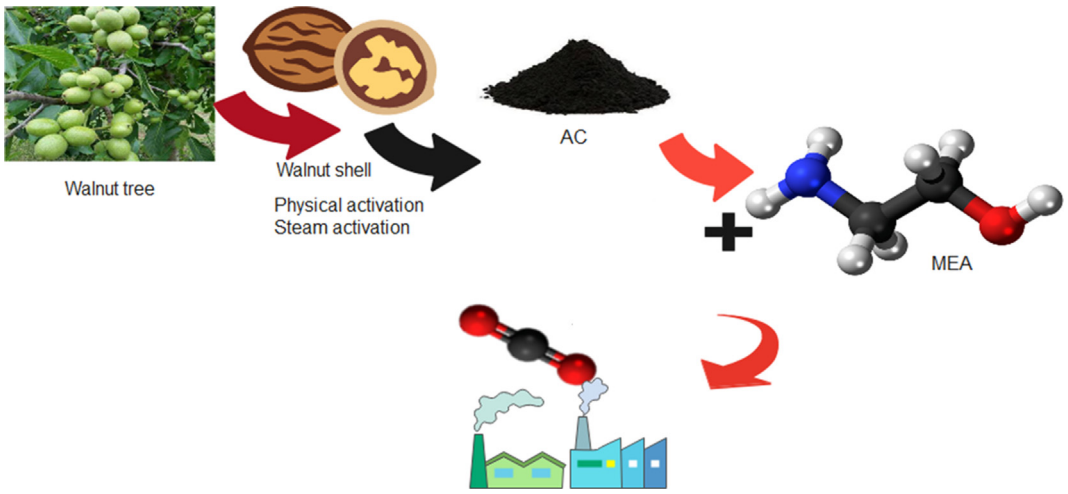

Figure 1. Experimental stages of the adsorbent preparation.

2.3. Absorption setup

The experiments of CO_2 absorption into MEA amine solution in presence of AC from waste walnut shell were carried out at a laboratory absorption setup. The schematic of absorption laboratory setup is presented in Figure 2. After the setup preparation, the adsorbent sample is placed inside the reactor and then the absorption process was started. The adsorbent samples were heated by nitrogen at 388 K for 1800 s before absorption experiments for dehumidification and finally vacuumed for 2400 s. When the reactor cools to ambient temperature, carbon dioxide is injecting into the reactor. Carbon dioxide was taken from a cylinder of high purity passes within pressure gauge and regulate to achieve wanted condition and it enters the mixing vessel under wanted pressure to regulate pressure of the reactor. A thermostat controls the temperature reactor, after which gas with the desired pressure from the mixing tank reaches the reactor, and the gas inlet valve is closed. Computer records all data obtained from the experiments (Khajeh and Ghaemi, 2020).

2.4. Experiments

As a result of homogenization, an aqueous solution with a specified weight percentage of MEA solvent (20 mL) is prepared and poured into the reactor tube with a certain amount of activated carbon. The temperature was adjusted using of a digital temperature controller. When the temperature reaches the desired value while the reactor outlet valve is open, pure CO_2 gas is passed through the reactor within a few seconds to remove the air reactor. The gas is then injected with the desired pressure into the reactor by closing the reactor outlet valve and opening the inlet valve. The amount of this gas can control through the inlet valve. After closing the reactor inlet valve, the stirrer turns on, stirrer speed is setting at 150 rpm in the all tests. The absorption process begins with a decrease in pressure over time until it reaches equilibrium. Equilibrium is achieving when the pressure remains constant. The experiments are performed for 1 h so that the equilibrium is reached at this time. Finally, after stabilizing the pressure and completing the adsorption process, the gas outlet valve was opened to remove the remaining CO_2 inside the chamber. Then, in the next step, the consumable solvent was removed by opening the chamber lid. This process is repeated by changing various parameters such as temperature, pressure, percentage of different weights of amine, and the amount of activated carbon to study the effect of operating parameters. In the reactor, the amount of CO_2 being injected (n_{CO2}) was calculated using the Peng-Robinson cubic equation of state. It has been determined that equilibrium pressure P_1 exists at equilibrium. As assumed that the vapor phase of CO_2 obeyed Dalton's law, the partial pressure of CO_2 in the vapor phase was calculated as follow (Khoshraftar et al., 2021; Tong et al., 2013).

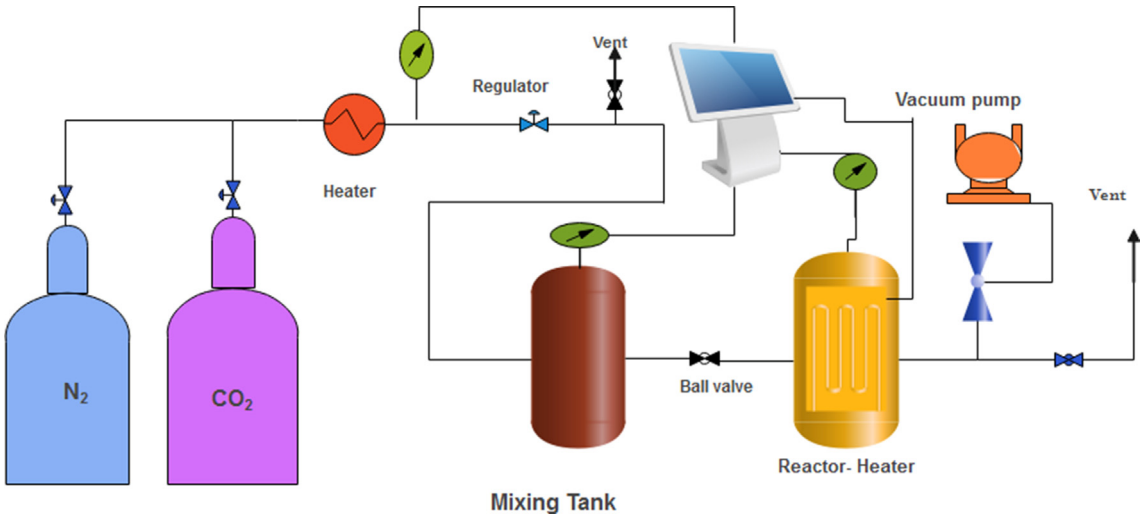

Figure 2. A schematic of absorption laboratory setup.

$$P_{CO2} = P_1 P_0 \quad (1)$$

The quantity of CO_2 $n^g_{CO_2}$ in the gas phase is calculated using Peng-Robinson cubic equation of state. Eq. (2) defines CO_2 loading as the mole of CO_2 absorbed per mole of adsorbent. In the liquid, n_{amine} denotes the mole number for amine solution (Tong et al., 2013).

$$CO_2 loading = \frac{n_{CO_2}}{n_{amine}} \quad (2)$$

Virial equation, assuming cut-off coefficients greater than the second order, was used to determine the compressibility factor.

$$Z = 1 + BP \quad (3)$$

$$\frac{BP_c}{RT_c} = F^{(0)}(T_R) + \omega F^{(1)}(T_R) \quad (4)$$

$$F^{(0)}(T_R) = 0.1445 - \frac{0.330}{T_R} - \frac{0.1385}{T_R^2} - \frac{0.0121}{T_R^3} - \frac{0.000607}{T_R^8} \quad (5)$$

$$F^{(1)}(T_R) = 0.0637 + \frac{0.331}{T_R^2} - \frac{0.423}{T_R^3} - \frac{0.008}{T_R^8} \quad (6)$$

B, P_c, T_c, and T_R are the second coefficient of virility, the critical pressure of CO_2, the critical temperature, and the decreased temperature, respectively. The coefficient of determination (R^2) is determined as follows:

$$R^2 = \frac{\sum_{i=1}^{n}(qe,mes - \overline{qe,mod})^2}{\sum_{i=1}^{n}(qe,mes - \overline{qe,mod})^2 + \sum_{i=1}^{n}(qe,mes - qe,mod)^2} \quad (7)$$

Modulus and mesindices refer to a model's predicted and measured absorption values, respectively, where n refers to the number of experimental data. In the experiments, $\overline{qe,mod}$ represents the average value (Khoshraftar et al., 2021). The percentage of CO_2 uptake and adsorption capacity is calculated using Eqs. (8) and (9) (Ramezanipour Penchah et al., 2021; Najafi et al., 2021).

$$Abs\,(\%) = (P_i - P_f)/P_i \times 100 \quad (8)$$

$$q = (m_i - m_f)/w = (VM_w/Rw)(P_i/Z_iT_i - P_f/Z_fT_f) \quad (9)$$

2.5. MEA–CO_2–H_2O system

The following reactions take place in the aqueous phase of MEA solution (Zheng et al., 2011). Chemical reactions in the absorption process increase the mass transfer and decrease the total pressure.

Water dissociation: $2H_2O \overset{K_1}{\leftrightarrow} H_3O^+ + OH^-$ (10)

CO_2 hydrolysis: $CO_2 + 2H_2O \overset{K_2}{\leftrightarrow} H_3O^+ + HCO_3^-$ (11)

Carbonate formation: $HCO_3^- + H_2O \overset{K_3}{\leftrightarrow} H_3O^+ + CO_3^{2-}$ (12)

MEA protonation: $H_3O^+ + MEA \overset{K_4}{\leftrightarrow} H_2O + MEAH^+$ (13)

Formation of MEA carbamate: $MEA + HCO_3^- \overset{K_5}{\leftrightarrow} MEACOO^- + H_2O$ (14)

2.6. CO_2 absorption mechanism in presence of activated carbon

A key role is played by functional groups on the surface of carbon materials. It is now common to use amine-based adsorbents as CO_2 capture statements due to their high adsorption capacities, rapid CO_2 adsorption rates, and simple regeneration properties. Activated carbon can be grafted with amine groups to enhance its ability to adsorb CO_2 in many different ways (Khoshraftar et al., 2021). As shown in Figure 3, CO_2 is absorbed into MEA solution via the absorption mechanism (Lv et al., 2015). The Molecular structure in CO_2 + H_2O + MEA is indicated in Figure 4.

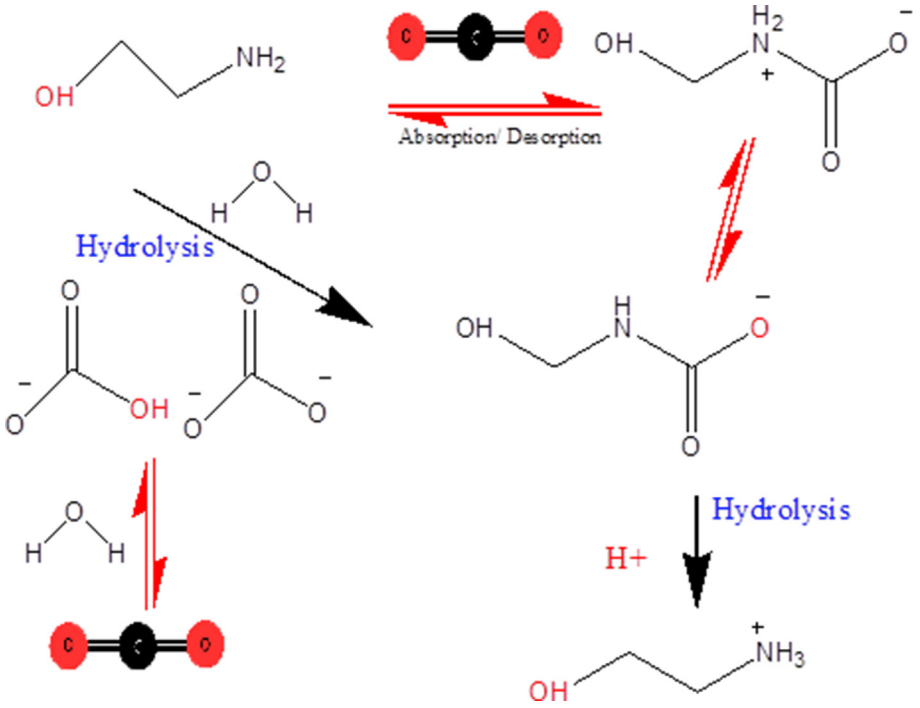

Figure 3. Mechanism of CO_2 absorption and desorption into MEA solution.

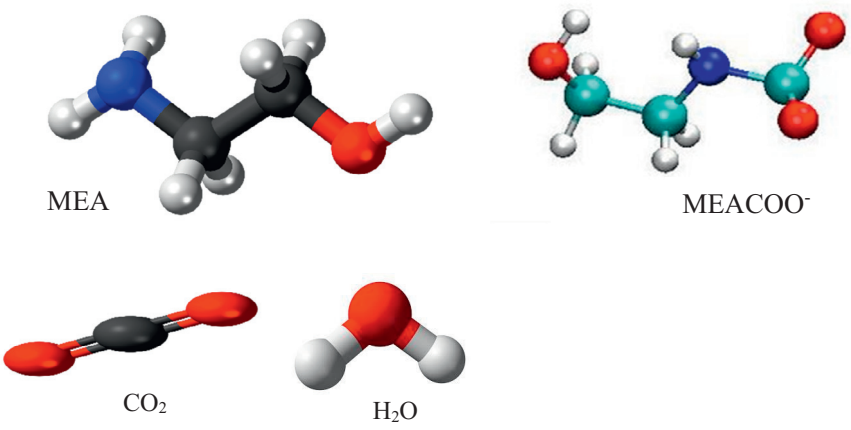

Figure 4. Molecular structures in MEA–CO_2–H_2O solution.

2.7. Design of experiment

This study aimed to provide experimental data on CO_2 uptake via MEA solution with and without AC. Therefore, the experimental data on loading, CO_2 uptake, and CO_2 uptake percentage in these solutions were measured. Whereas in recent years, the RSM has attracted much attention among researchers as an efficient method for optimization, to reduce the number of the experimental data, it was designed using the RSM method and based on a central composite design (Ghaemi et al., 2021; Khoshraftar et al., 2021; Pashaei et al., 2020). RSM is a statistical method used to design and analyze empirical data. RSM with CCD is an effective method for empirically understanding the relationship between the examined parameters and the system response. RSM helps to analyze the interactions between different parameters, reduce time and cost, provide an optimal overall response, and show a table of selected parameters and ranges (Saeidi et al., 2018; Behroozi et al., 2020). The main operating parameters, including temperature, pressure, concentrations of chemical solvents, and activated carbon concentrations, affect the CO_2 uptake process. In design of the experiments, suitable conditions for CO_2 removal using chemical solvents in the presence of solid particles have been considered. The range of operational variables is selected based on the literature, the results of preliminary experiments, and the existing setup. The tests required by CCD is two-dimensional factorial, two-dimensional axial, and NC center point. The number of parameters in each test determines k. For comparability, the design presented in 5 levels $\alpha\ +,\ 1\ +,\ 0,\ 1,\ \alpha-$ where α is equal to $(2k)^{0.2}$. This feature ensures a constant variance at points that are at a constant distance from the center points and provides equal accuracy in estimating the response in each direction of the design (Leonzio, 2017). Input parameters and response are correlated as follows:

$$y = f(x_1, x_2, \ldots, x_k) + \varepsilon \tag{15}$$

According to the relation (15) y to the input parameters x_1, x_2,… x_k depends, and the remaining parameter is related to the experiments. For RSM, the quadratic polynomial formula is the most common model used to match experimental data. Accordingly, experimental data was used to develop a quadratic polynomial model according to the following equation:

$$y = \beta_0 + \sum_{i=1}^{k} \beta_i X_i + \sum_{i=1}^{k} \sum_{j=1}^{k} \beta_{ij} X_i X_j \sum_{i=1}^{k} \beta_{ii} X_i^2 + \varepsilon \tag{16}$$

In Eq. (16), β_0 represents a constant time, $\beta_j$and β_i represent coefficients of linear parameters, β_{ij} represents coefficient of interactive parameters, β_{ii} and β_{ij} represents coefficients of the quadratic parameters, and finally ε describes the remaining error. The values of the center point are used to estimate the coefficients of the degree terms. The axial points (located at an alpha distance from the center point) are used to estimate the coefficients of the degree terms. The factorial points (located in the center of the cube with side length equal to 2) are used to estimate linear term coefficients (Ghaemi et al., 2021; Khoshraftar et al., 2021; Leonzio, 2017). In this study, experiments were designed with temperature, pressure, amount of activated carbon, and MEA concentration. Responses including CO_2 loading (molCO_2/mol MEA), amount of CO_2 absorbed in terms of (mol/L), and percentage of CO_2 absorption (%). The process experiments were carried out at temperature in range of 20–60 °C, activated carbon in range of 0–0.9 g/L, pressure in range of 3.5–9.5 bar, and MEA concentrations in range of 2.5–8.5 wt%.

2.8. Experiments

The operating parameters including temperature, pressure, and concentration of MEA, and amount of activated carbon are presented in Table 2. In the RSM modeling, the central composite design was used for each parameter with 5 levels. All tests include 30 runs containing six replicates for the focal point.

3. Results and discussion

3.1. Response surface methodology

The RSM was used to investigate the impact of some variables on CO_2 absorption. The different values that should be calculated by the experiments are known as independent level variables. To predict and select influential factors on the CO_2 absorption parameter, the quadratic regression model was applied for the response obtained onto 30 run experiments (Table 3). Table 4 displays the modeling results using coded factors to express the coefficients.

3.2. Variance analysis (ANOVA)

Analysis of variance is a statistical method that examines the level of significance and importance of the whole model (Khoshraftar et al., 2021; Pashaei et al., 2020). ANOVA analysis shows whether the difference due to the model is significant compared to the differences in error remaining from the experimental data. These results were obtained from the information given in the p-value column of Table 5. For p-values less than 0.05 and 0.001, the model terms are very considerable, respectively. Because this value is less than the value of 0.05, this indicates the significance of the

Table 2. Overview of three independent variables, including levels of each.

Parameters	Name	Unite	Low level	Upper level
T	A	°C	20	60
P	B	Bar	3.5	9.5
C_{MEA}	C	Wt%	2.5	8.5
m_{AC}	D	g/L	0.3	0.9

Table 3. The effectiveness of absorption experiments based on the design and response.

STD	Run	Factor 1	Factor 2	Factor 3	Factor 4	Response 1	Response 2	Response 3
		A:T	B: P	C: C amine	D: m	R	Loading	C_{CO2}
		°C	bar	w%	g	-	Cco_2/C_{MEA}	mol/L
21	19	40	6.5	2.5	0.60	19.54	0.7	0.294
3	9	30	8.0	4.0	0.45	19.76	0.7	0.428
2	10	50	5.0	4.0	0.45	27.47	0.5	0.341
1	27	30	5.0	4.0	0.45	29.86	0.6	0.389
4	30	50	8.0	4.0	0.45	19.32	0.6	0.378
12	2	50	8.0	4.0	0.75	19.78	0.6	0.395
9	15	30	5.0	4.0	0.75	33.24	0.6	0.406
10	25	50	5.0	4.0	0.75	29.23	0.6	0.362
11	29	30	8.0	4.0	0.75	21.10	0.7	0.438
23	13	40	6.5	5.5	0.30	31.12	0.5	0.454
26	1	40	6.5	5.5	0.60	31.70	0.6	0.503
17	6	20	6.5	5.5	0.60	33.60	0.6	0.537
20	7	40	9.5	5.5	0.60	24.20	0.6	0.544
30	8	40	6.5	5.5	0.60	33.53	0.6	0.500
28	11	40	6.5	5.5	0.60	33.15	0.6	0.496
25	14	40	6.5	5.5	0.60	30.67	0.6	0.498
19	18	40	3.5	5.5	0.60	49.25	0.5	0.462
29	20	40	6.5	5.5	0.60	31.70	0.6	0.503
18	22	60	6.5	5.5	0.60	28.41	0.4	0.402
27	23	40	6.5	5.5	0.60	29.67	0.5	0.491
24	4	40	6.5	5.5	0.90	33.71	0.6	0.512
7	3	30	8.0	7.0	0.45	26.62	0.6	0.633
8	5	50	8.0	7.0	0.45	27.81	0.5	0.531
6	21	50	5.0	7.0	0.45	42.86	0.4	0.507
5	26	30	5.0	7.0	0.45	49.50	0.5	0.586
16	12	50	8.0	7.0	0.75	28.41	0.5	0.559
14	17	50	5.0	7.0	0.75	43.58	0.5	0.519
13	24	30	5.0	7.0	0.75	51.25	0.5	0.596
15	28	30	8.0	7.0	0.75	30.57	0.6	0.657
22	16	40	6.5	8.5	0.60	46.18	0.5	0.687

A: Temperature; B: Pressure; C: Concentration of amine; D: amount of activated carbon; C_{CO2}: the amounts of CO_2 absorption (mol/L); %R: %Removal.

Table 4. Estimated Factors based on coding coefficients.

Factor	Coefficient Estimate	df	Standard Error	95% CI Low	95% CI High	VIF
Intercept	0.5568	1	0.0028	0.5509	0.5627	
A-T	-0.0374	1	0.0014	-0.0403	-0.0344	1.00
B–P	0.0230	1	0.0014	0.0200	0.0259	1.00
C-Camin	-0.0530	1	0.0014	-0.0560	-0.0501	1.00
D-m	0.0115	1	0.0014	0.0086	0.0145	1.00
AB	-0.0023	1	0.0017	-0.0059	0.0013	1.00
AC	-0.0014	1	0.0017	-0.0051	0.0022	1.00
AD	0.0013	1	0.0017	-0.0023	0.0049	1.00
BC	-0.0043	1	0.0017	-0.0079	-0.0007	1.00
BD	0.0007	1	0.0017	-0.0029	0.0043	1.00
CD	-0.0022	1	0.0017	-0.0058	0.0014	1.00
A^2	-0.0092	1	0.0013	-0.0119	-0.0064	1.05
B^2	0.0002	1	0.0013	-0.0025	0.0030	1.05
C^2	0.0121	1	0.0013	0.0093	0.0149	1.05
D^2	-0.0065	1	0.0013	-0.0093	-0.0038	1.05

model. The model terms with a p-value greater than 0.1 are not noteworthy. Nonsense lack of fit that the distance between the actual values and the forecast is small. As a general rule, p-value values less than 0.05

Table 5. Analyzing variance (ANOVA) of a quadratic response surface.

Source	Sum of Squares	df	Mean Square	F-value	p-value
Model	0.1261	14	0.0090	195.29	<0.0001
A-T	0.0335	1	0.0335	726.79	<0.0001
B–P	0.0127	1	0.0127	274.24	<0.0001
C-Camin	0.0675	1	0.0675	1463.80	<0.0001
D-m	0.0032	1	0.0032	69.31	<0.0001
AB	0.0001	1	0.0001	1.85	0.1933
AC	0.0000	1	0.0000	0.7168	0.4105
AD	0.0000	1	0.0000	0.5975	0.4515
BC	0.0003	1	0.0003	6.45	0.0226
BD	7.563E-06	1	7.563E-06	0.1639	0.6913
CD	0.0001	1	0.0001	1.66	0.2172
A^2	0.0023	1	0.0023	49.85	<0.0001
B^2	1.313E-06	1	1.313E-06	0.0285	0.8683
C^2	0.0040	1	0.0040	86.97	<0.0001
D^2	0.0012	1	0.0012	25.36	0.0001
Residual	0.0007	15	0.0000		
Lack of Fit	0.0005	10	0.0000	0.9485	0.5610
Pure Error	0.0002	5	0.0000		
Cor Total	0.1268	29			

indicate that the parameter is significant, and on the other hand, p-value values greater than 0.1 indicate a lack of significance (Gholamiyan et al., 2020). As shown in Table 5, the p-value is less than 0.001, which indicates that the terms of the model are of great importance. According to the p-value column, terms A, B, C, D, AC, A^2, and D^2 are considerable terms and affect the response variables significantly. Fortunately, for R^2_{adj} and R^2_{pred} to be satisfactory for the quadratic model, they are equal to 0.9932 and 0.9815, which are within the desired range (>0.5). Also, due to their difference of less than 0.2, they agree with each other. The closer R^2 is to 1, the better for the designed model. The value of R^2 for our model is 0.9945, which is reasonable. A value of R^2 0.9945 indicates the high correlation between the observed and predicted values of the model, which confirms the model accuracy (Khoshraftar et al., 2021).

The model used in the central composite design is a quadratic model that, in addition to considering the principal factors and the binary interaction of the factors, considered the second degree of the factors. The obtained equation describes the response behavior in the experimental range as a function of independent variables.

$$\begin{aligned} CO_2Loading = {} & 0.549903 - 4.992 \times 10^{-3}T + 0.031806P - 0.069917C_{MEA} \\ & + 0303889m_{AC} - 0.154 \times 10^{-4}T \times P + 0.96 \times 10^{-4}T \\ & \times C_{MEA} + 0.875 \times 10^{-3}T \times m_{AC} - 1.1917 \times 10^{-3}P \times C_{MEA} \\ & + 3.056 \times 10^{-3}P \times m_{AC} - 9.722 \times 10^{-3}C_{MEA} \times m_{AC} - 0.97 \\ & \times 10^{-4}T^2 - 0.125 \times 10^{-3}P^2 + 5.153 \times 10^{-3}C_{MEA}^2 \\ & - 0.179167{m_{AC}}^2 \end{aligned} \quad (17)$$

In Figure 5a, the residual normal probability reflects the difference between expected and observed responses. The normal probability graph versus extremely studentized residuals was usually positioned on a straight line and typically distributed, as seen in this diagram. Figure 5b depicts the actual versus expected value plot for CO_2 uptake efficiency increase. The residuals were usually positioned on a straight line and typically distributed, as seen in this diagram. For all responses, the actual and expected values were similar to each other. As a result of this finding, these models were suitable for empirical data and can be used to evaluate and predict absorption efficiency. It is preferable to have a ratio or sufficient precision higher than 4 (In this study: Adeq precision = 57.47). The proposed model is basing on the results of the ANOVA study and Figure 6b. As is well documented, least-squares residuals are a tool for evaluating model adequacy. Figure 6a depicted the hypothesis of constant variance at different levels by plotting the expected response values versus the residual obtained from the model. There was a random distribution of the x-axis between +3.879 and -3.879, as seen in these graphs, with no discernible patterns. The pattern was not inconsistent with the assumptions of constant variance and independence, as can be seen. As in Figure 6b, difference in fits metric is dependent on the difference in fitting between the expected value of each run as a result of removing each run. Since all of the run residues were on or near the ranges of −2.121 to 2.121, there was no discernible trend.

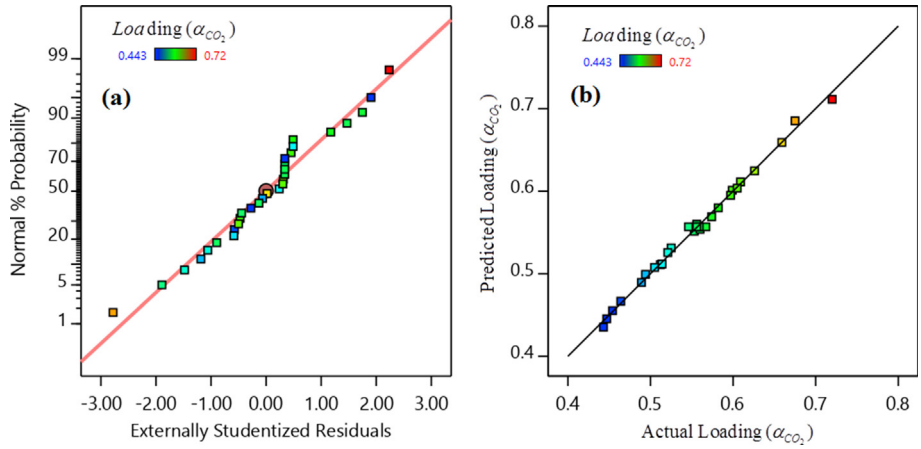

Figure 5. a) Standard residuals-based normal graph, b) A graph comparing predicted CO2 removal efficiency values with experimental (actual) values.

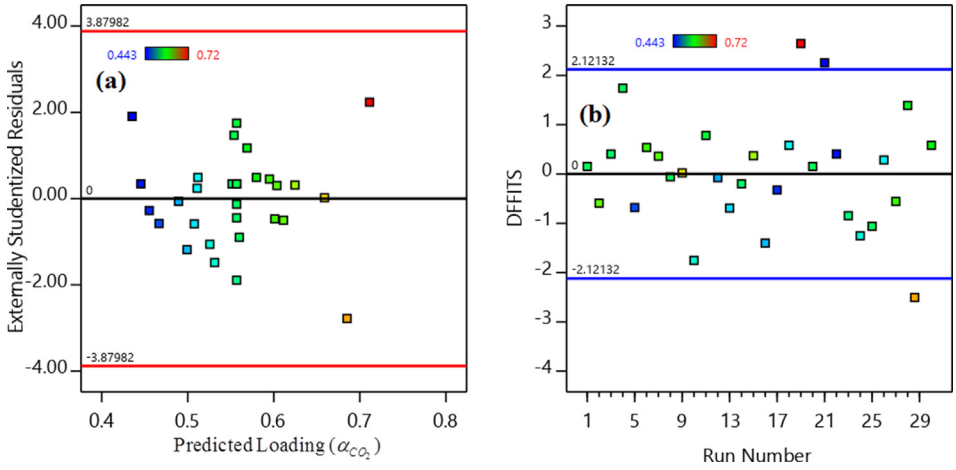

Figure 6. (a) Residuals with an external studentization, (b) No. of runs.

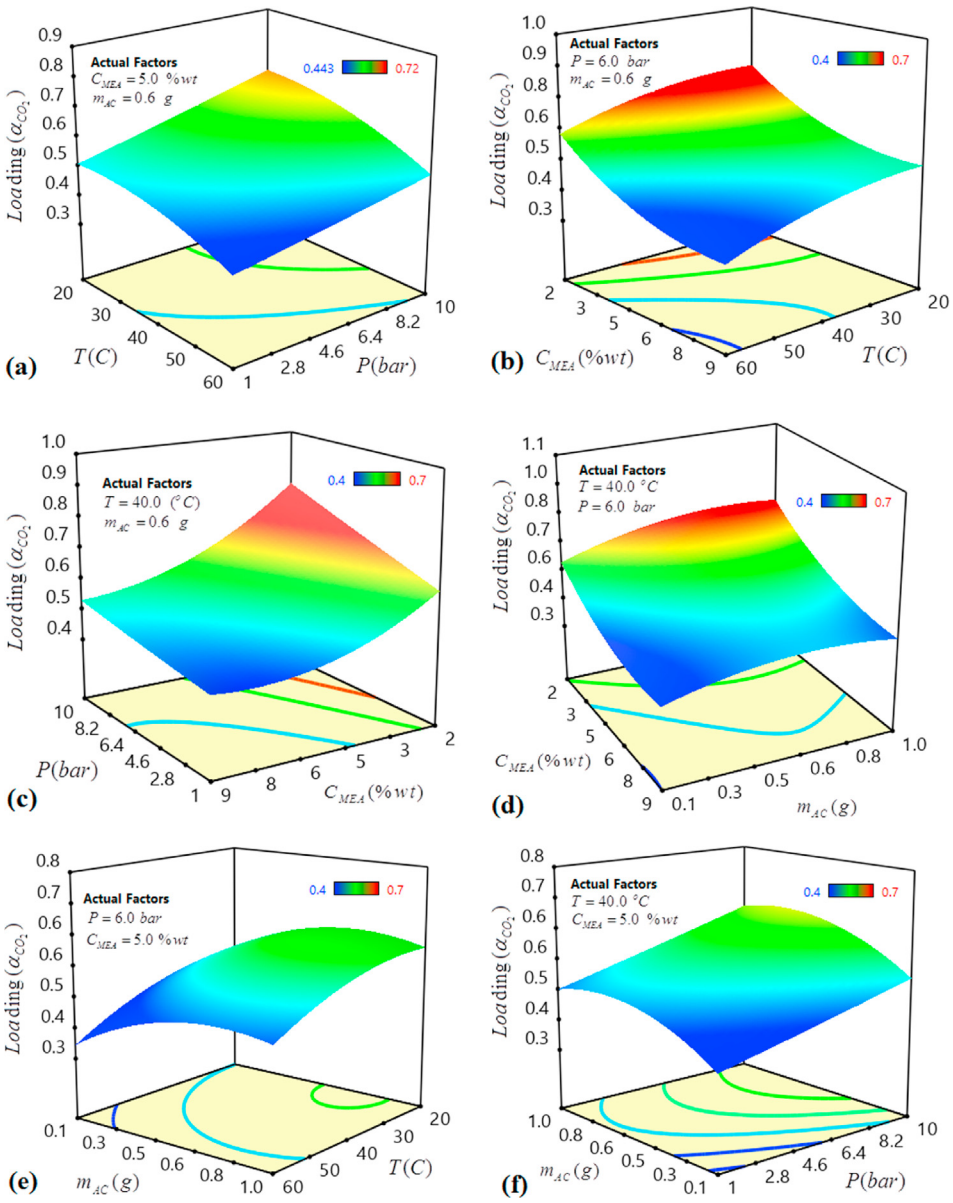

Figure 7. 3D plot response surface of CO_2 loading a) Interaction of temperature and pressure on CO_2 loading; b) Interaction of wt% C_{MEA} and temperature on CO_2 loading; c) Interaction of pressure and wt% C_{MEA} on CO_2 loading; d) Interaction wt% C_{MEA} and m_{AC} on CO_2 loading; e) Interaction of m_{AC} and temperature on CO_2 loading; f) Interaction of m_{AC} and pressure on CO_2 loading.

3.3. Analysis of response surface

The three-dimensional response surfaces graphs for CO_2 loading were depicted in Figure 7. According to Figure 7a, a rise in pressure at constant temperature and a decrease in temperature at constant pressure increase CO_2 loading. The two variables of T and P show that a rise in pressure and a decrease in temperature result in a significant increase in CO_2 loading (Khoshraftar et al., 2021). According to Figure 7b, a decrease in the concentration of MEA (wt%) and decrease temperature increase CO_2 loading. The relationship between the process pressure and MEA concentration is shown in Figure 7c. According to Figure 7c, a rise in pressure and a decrease in concentration increase CO_2 loading. The effect of MEA concentration on CO_2 loading was to be greater than the pressure (Khoshraftar et al., 2021). The relationship between the amount of active carbon (g) and MEA concentration (wt%) variables is shown in Figure 7d. According to Figure 7c, an increase in the amount of active carbon and a decrease in concentration, increasing CO_2 loading. The relationship between the temperature and the amount of active carbon (g) is presented

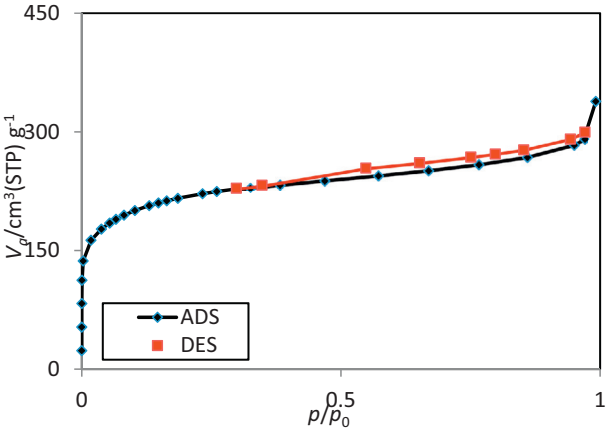

Figure 8. N_2 adsorption/desorption isotherm on activated carbon at 77 K.

in Figure 7e. An increase in carbon amount and a decrease in temperature result in a rise in CO_2 loading in Figure 7e. The effect of the process temperature on CO_2 loading was to be greater than the amount of active carbon. The relationship between the amount of active carbon (g) and pressure is shown in Figure 7f. According to Figure 7f, a rise in the amount of active carbon and pressure increasing CO_2 loading. It has been found that the process pressure has greater effects than the amount of activated carbon on CO_2 loading.

3.4. Adsorption/desorption isotherm

Nitrogen adsorption/desorption isotherms were measured on a Micromeritics ASAP 2020 (USA) adsorbent. Before measurement, all samples were evacuated and reduced at 180 °C for more than 6 h under high vacuum conditions. The AC from walnut shell surface area was calculated applying the BET method from the absorption radius in the relative pressure range (p/p_0 0.01 to 0.2) (Figures 8 and 9). Pore size distribution by the adaptive nonlinear density function method was determined using nitrogen adsorption. The total pore volume of *Vtot* was estimated according to the amount of adsorption at p/p_0. The isothermal distributions of N_2 adsorption was calculated at 77 K. The adsorption reaction of carbon dioxide and carbon has a van der Waals force, and for the study of BET, it is important to pay attention to this issue in the analysis. The higher pores introduced the greater absorption capacity (Khoshraftar and Shamel, 2016). The shape of the gas isotherm shows the amount absorbed at a certain relative pressure. According to Figure (8), the N_2 adsorption isotherm corresponds to the type IV that is classified as the International Union of Pure and Applied Chemistry (IUPAC) and is also known as mesoporous material. Therefore, it is in accordance with the IUPAC standard, which fixes the expanded width of the mesoporous material in the range of 2–50 nm (Ghaemi et al., 2021). The total pore volumes ($P/P_0 = 0.990$) was 0.4863 cm^3g^{-1} and the specific Brunauer-Emmett-Teller (BET) surface areas (SBET) was 881.84 m^2g^{-1}.

3.5. Pressure effect on CO2 absorption

For evaluating the effect of pressure on CO_2 loading, the same conditions are selected as 5.5 wt% of MEA, 0.6 g of activated carbon, and 313 K at pressures of 3.5, 6.5, and 9.5 bar Figure 10 shows the loading of CO_2 against time. The amount of carbon dioxide loading reached a maximum at a pressure of 9.5 bar. It is clear that the load and the amount of mole absorbed by CO_2 increase with increasing CO_2 pressure (Khoshraftar et al., 2021). Increasing the CO_2 pressure increases the amount of CO_2 present in the inlet stream. Figure 11 illustrates the impact of CO_2 loading

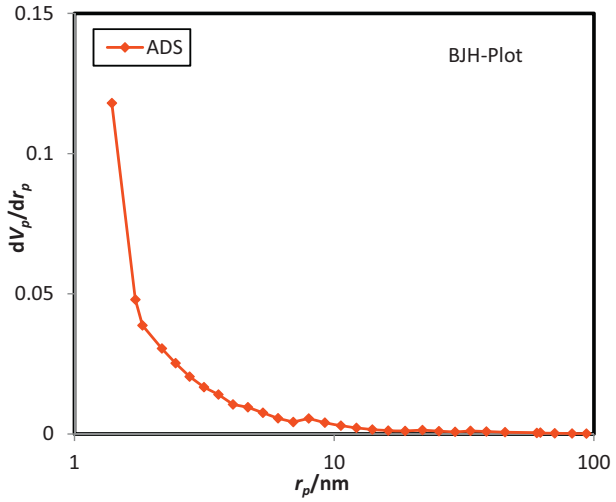

Figure 9. Pore size distribution of the activated carbon by BJH method due to pore area.

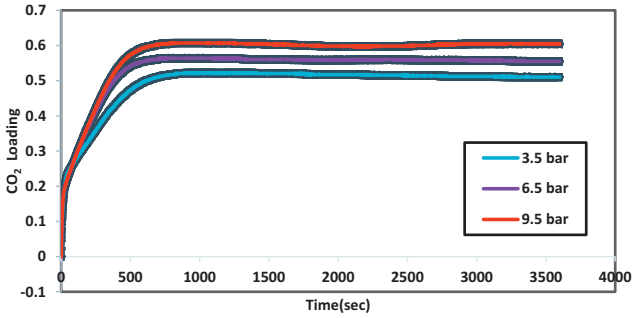

Figure 10. Pressure effect on CO_2 loading in MEA solution at 40 °C, 5.5 wt% of MEA solution, and activated carbon of 0.6 g/L.

under different pressure conditions with and without activated carbon. It is noted that by adding 0.6 g of the activated carbon at different pressures, the CO_2 loading increases. Because of the greater solubility of carbon dioxide in amine solutions, the chemical equilibrium reaction towards the right occurs (Behroozi et al., 2020, 2021).

3.6. Effect of tempressure

Figure 12 shows the effect of temperature (293, 313, and 333 K) on CO_2 loading in MEA solution of 5.5 wt% and 0.6 g/L of activated carbon at a pressure of 6.5 bar Figure 13 shows the effect of temperature on CO_2 loading. According to the obtained results, the highest CO_2 loading is related to temperature of 293 K. The results show that increasing the temperature has a negative effect on CO_2 loading, and CO_2 uptake gradually decreases. Therefore, it is concluded that desorption phenomenon has occurred at 333 K. Increased operating temperatures result in reduced CO_2 uptake because adding heat causes the CO_2 molecules to be motivated, causing the unstable molecules to form in the system (Rashidi and Yusup, 2017). The same results are presented in the literature (Karbalaei Mohammad et al., 2020; Khoshraftar et al., 2021). Figure 13 shows the effect of temperature on CO_2 loading in the presence of AC from the waste walnut shell at different temperatures. As shown in Figure 13, adding 0.6 g of activated carbon to MEA solution has a good effect on CO_2 absorption. Increasing temperatures and exothermic interactions lower the physical solubility of the gas in amine solutions (Khoshraftar et al., 2021).

3.7. Effect of concentration

Figures 14 and 15, show the effect of MEA concentration on CO_2 loading and uptake at MEA concentrations of 2.5, 5.5, and 8.5 wt%, respectively. According to Figure 14, with increasing MEA

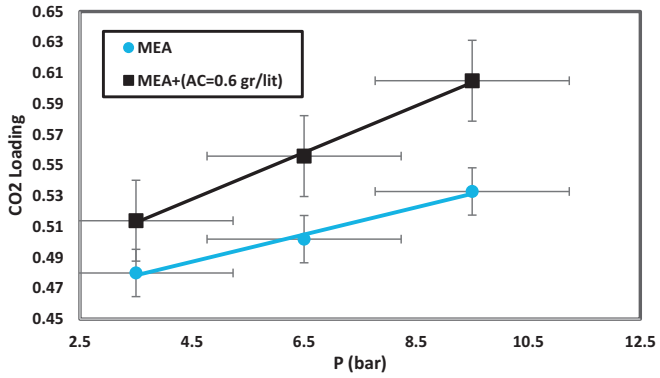

Figure 11. CO_2 loading in MEA solution with and without AC in 5.5 wt% solvent at 40 °C and pressures of 2.5–9.5 bar.

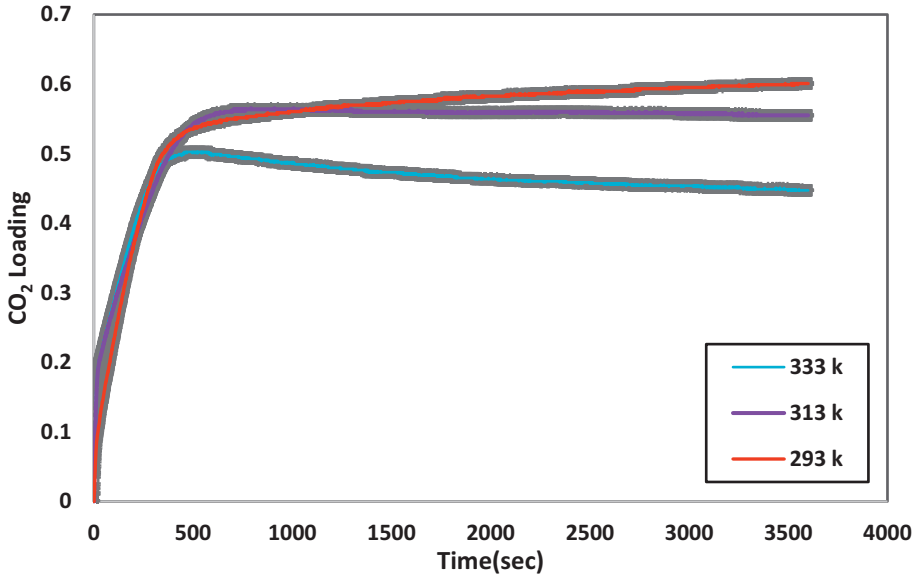

Figure 12. Effect of temperature on CO_2 loading at 6 bar, 5.5 wt% of MEA solution, and activated carbon of 0.6 g/L.

concentration, the CO_2 loading decreases, but according to Figure 15, increasing MEA concentration, the amount of mole absorbed CO_2 increases. Therefore, as the percentage of MEA concentration increases, it absorbs more moles of CO_2 and increases the amount of absorption percentage (Khoshraftar et al., 2021). This increase in the absorption of moles of CO_2 was not enough to overcome the increase in adsorbent concentration. Therefore, CO_2 loading decreases with increasing MEA concentration. The reason for the increase in CO_2 loading at MEA concentration of 2.5 wt% is the significantly lower solvent concentration and consequently the higher CO_2 loading in these conditions. It is

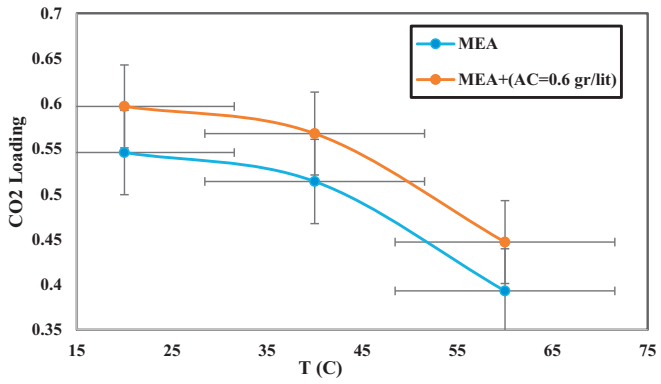

Figure 13. Temperature effect of CO_2 loading in presence of AC, at pressure of 6.5 bar and 5.5 wt% of MEA.

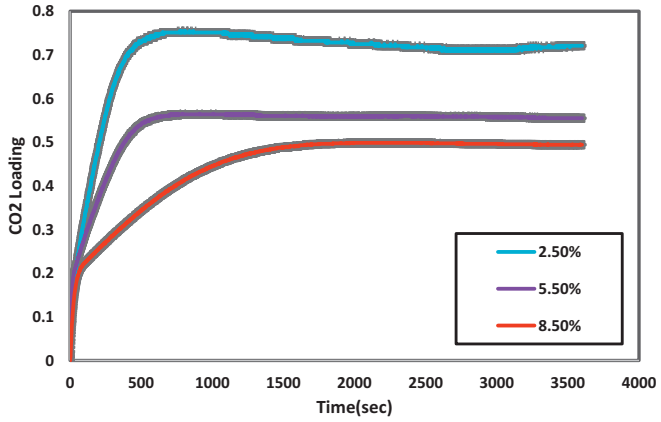

Figure 14. CO_2 loading at different concentrations of MEA at 40 °C, P: 6.5 bar and amount of activated carbon 0.6 g/L.

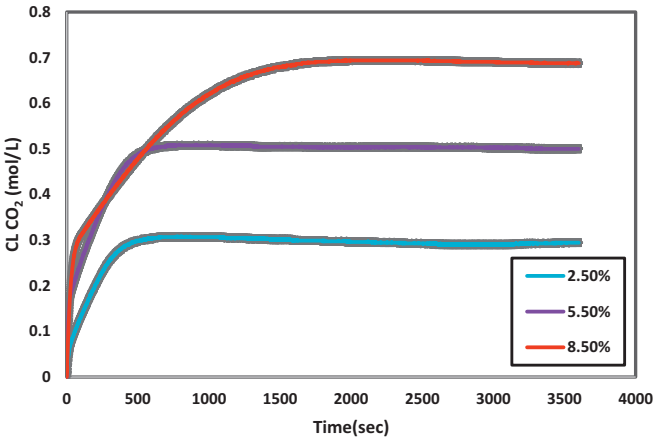

Figure 15. Effect of MEA concentration on CO_2 uptake at 40 °C, activated carbon of 0.6 g/L, and pressure of 6.5 bar.

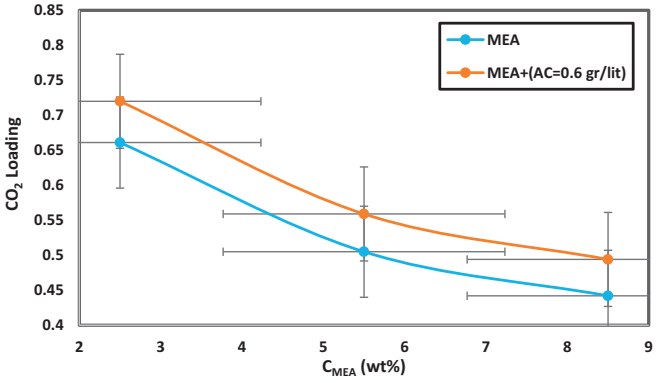

Figure 16. CO_2 loading with vs MEA solution at temperature of 40 °C and pressure of 6.5 bar.

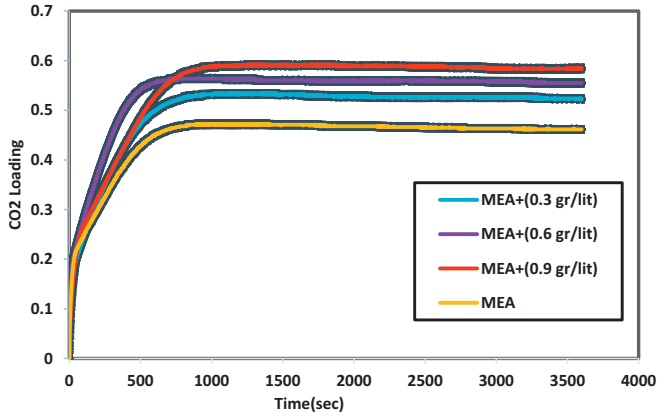

Figure 17. The effect of activated carbon and absorption time on CO_2 loading at pressure of 5 bar and MEA of 5.5 wt% and temperature of 40 °C.

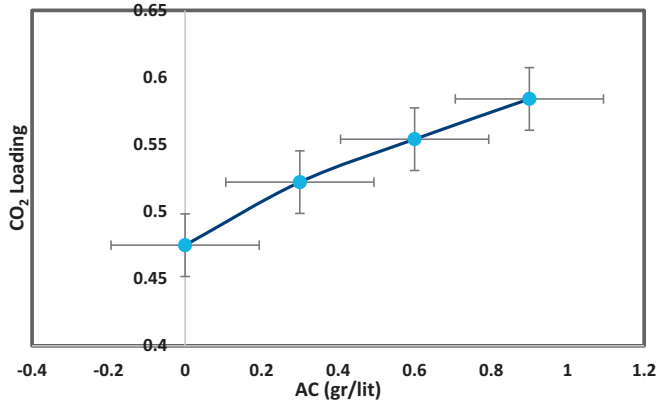

Figure 18. The effect of activated carbon content on carbon dioxide loading at pressure of 5 bar; MEA of 5.5wt% and temperature of 40 °C.

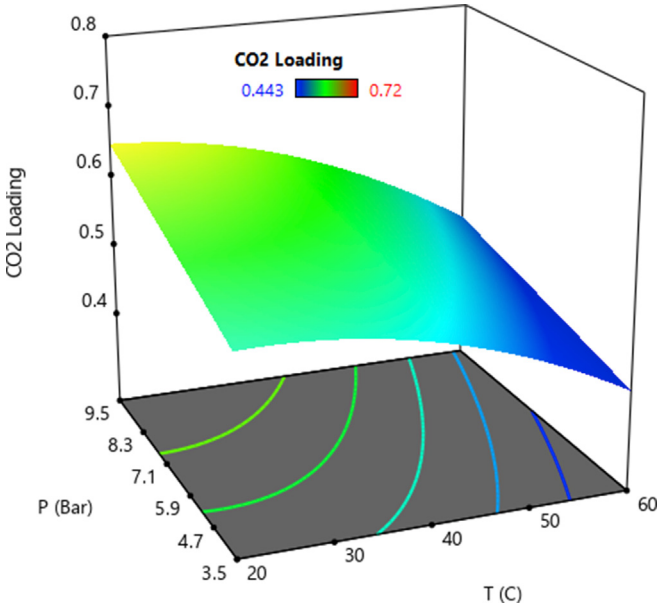

Figure 19. CO_2 loading in MEA solution in the presence of activated carbon in terms of temperature and pressure at MEA concentration of 5.5 wt% and activated carbon of 0.6 g/L.

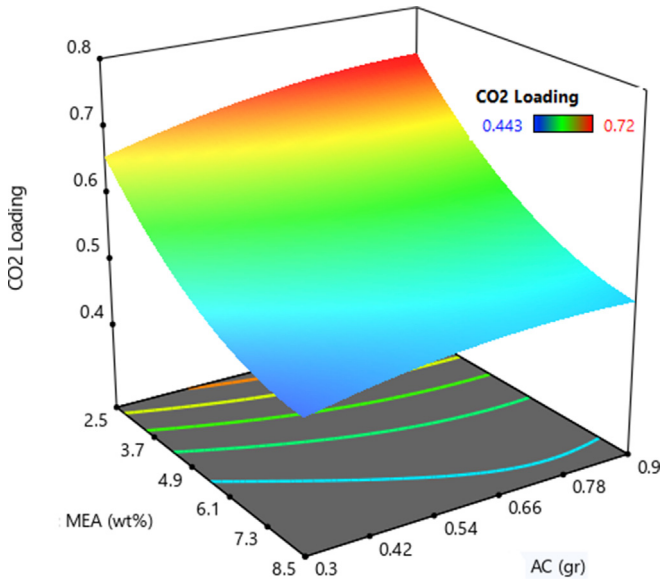

Figure 20. Effect of MEA concentration and activated carbon amount on CO_2 loading.

Table 6. An overview of the process factors and responses.

Name	Goal	Lower Limit	Upper Limit	Lower Weight	Upper Weight	Importance
A:T	is in range	30	50	1	1	3
B:P	is in range	5	8	1	1	3
C:Camin	is in range	4	7	1	1	3
D:m	is in range	0.45	0.75	1	1	3
R	maximize	19.32	51.25	1	1	5
Loading	maximize	0.443	0.72	1	1	5
Cco_2	maximize	0.294	0.687	1	1	5

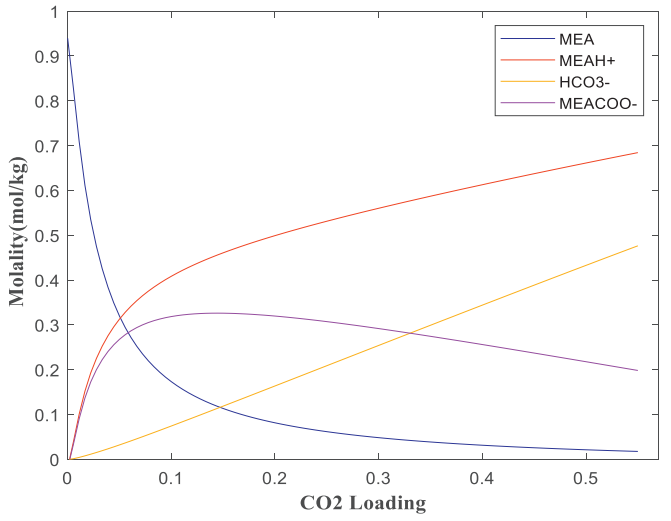

Figure 21. Concentration of ionic and molecular components in MEA–CO_2–H_2O system at 313 K, MEA concentration of 0.9 mol/kg, and activated carbon of 0.6 g/L.

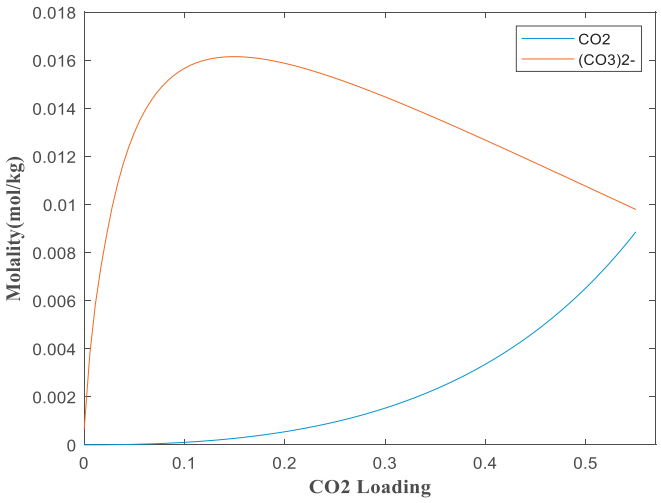

Figure 22. Concentration of ionic and molecular components in the $CO_2 + H_2O$ + MEA system at temperature of 313 K, 0.9 mol/kg MEA solution, and 0.6 g/L activated carbon.

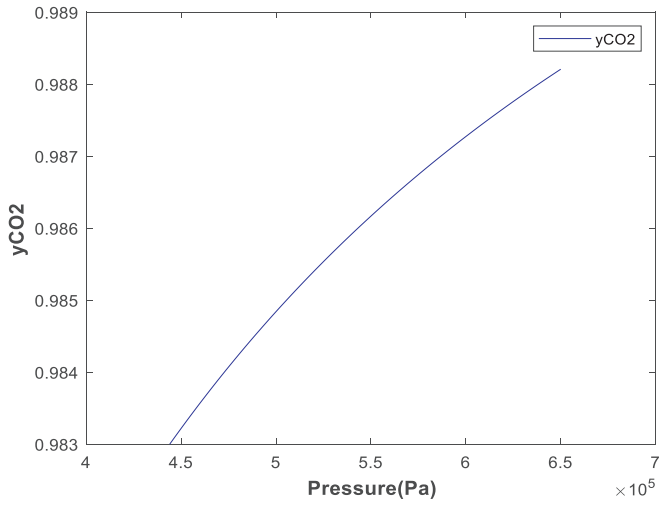

Figure 24. Mole fraction of CO_2 in the gas phase in MEA–CO_2–H_2O system at 40 °C, pressure of 6.5 bar, MEA concentration of 5.5 wt%, and activated carbon of 0.6 g/L.

clear that CO_2 loading is increased at all different MEA concentration in presence of AC (see Figure 16).

3.8. Effect of absorbent dosage

Figures 17 and 18 evaluate the effect of activated carbon in MEA solution of 5.5 wt% on CO_2 loading. In the experiments, activated carbon dosage was used in range of 0–0.9 g/lit. It is clear that the inclusion of AC from waste walnut shell in the MEA solution increased the CO_2 loading. According to the literature, addition of solid particles to chemical solutions enhanced the mass transfer of CO_2. The most effective particle is activated carbon, as proven by experiments. In terms of solid particle adsorption, the selection of the chemical solution is a significant factor (Khoshraftar et al., 2021; Mannel et al., 2017).

3.9. Evaluating the RSM parameters

The response surface draws a polynomial diagram of two degrees while the two fixed variables and the other two variables are within the

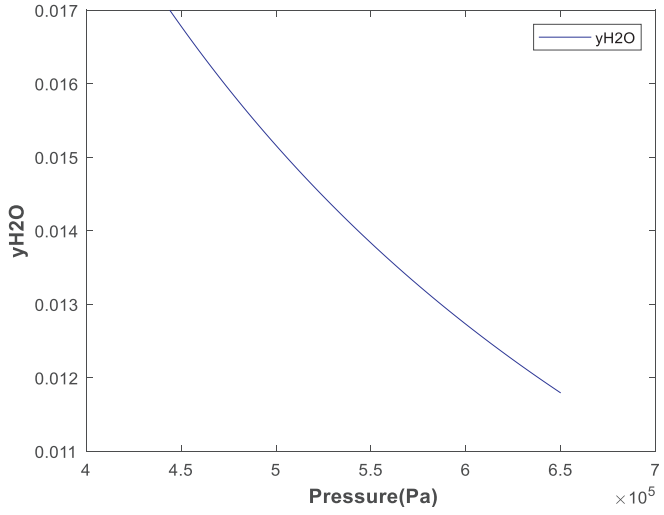

Figure 25. Water mole fraction in the gas phase in MEA–CO_2–H_2O system at temperature of 40 °C, pressure of 6.5 bar, MEA concentration of 5.5 wt%, and activated carbon of 0.6 g/L.

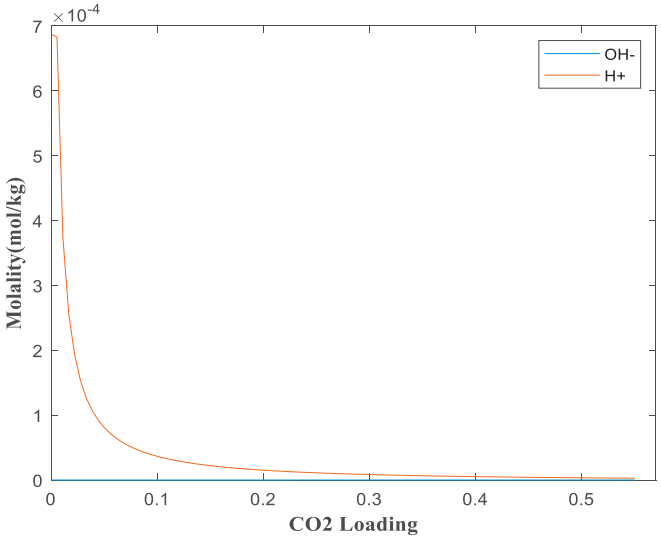

Figure 23. Concentration of ionic and molecular components in the MEA–CO_2–H_2O system at temperature of 313 K, 0.9 mol/kg MEA solution, and 0.6 g/L activated carbon.

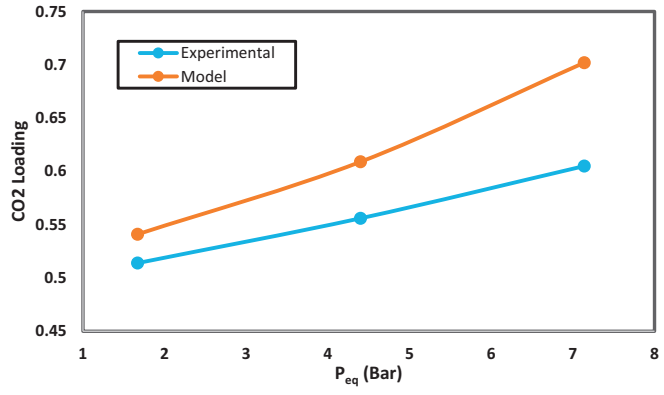

Figure 26. Comparison of experimental and modeling of MEA-CO_2 –H_2O system at temperature of 40 °C, MEA concentration of 5.5 wt% and activated carbon of 0.6 g/L.

Table 7. Comparison of experimental and modeling result of MEA-CO_2 –H_2O system at temperature of 40 °C, MEA concentration of 5.5 wt% and activated carbon of 0.6 g/L.

Erorr (%)	Pexp (Bar)	P_{eq} (Bar)	α_{exp}	α_{model}
5.12	3.50	1.67	0.514	0.541
8.73	6.5	4.40	0.556	0.609
13.86	9.50	7.14	0.605	0.702

Table 8. Optimization of the process parameters.

Parameters	The optimum values
T (°C)	30.00
P (bar)	5.19
C_{amine} (wt%)	7.00
M_{AC} (g/L)	0.75

experimentally defined range. In this section, the effects of operational parameters on CO_2 loading and interactions between variables are indicated in 3D diagrams. Figures 19 and 20 show the three-dimensional diagrams of CO_2 loading as a function of operating conditions. Figure 19 shows the effect of temperature and pressure, on CO_2 loading. According to Figure 20, CO_2 loading increases with increasing amount of activated carbon.

RSM is a common optimization method used to determine the optimal values of variables for the best CO_2 loading response (Ghaemi et al., 2021; Pashaei et al., 2017). The quadratic equation is optimized to achieve the maximum CO_2 uptake in the predetermined experimental range. The optimum parameters of the CO_2 absorption process are obtained from numerical optimization using experimental design and including temprature of 303 K; pressure of 5.193 bar; C_{MEA} of 7 wt%; m_{AC} of 0.75 g/L; loading of 0.527 $molco_2/mol_{amin}$. The selection of numerical optimization was based on reducing energy use and reducing process costs. Table 6 shows the ranges of both factors and responses for the process optimization.

3.10. Component concentrations in the liquid bulk

The Pitzer model was used for modeling of MEA–CO_2–H_2O system. In the modeling equations of chemical reactions equilibrium, mass balance, charge balance, and phase equilibrium were solved simultaneously. The concentrations of all components in the system are unknown and are defined as independent variables (Bougie and Iliuta, 2011; Wagner et al., 2013). According to the attached Table No.1, eight equations including five equilibrium equations of chemical reactions, two equilibrium equations of mass, and one equilibrium equation of charge are solved simultaneously. The reaction of MEA with CO_2 caused a sharp decrease in MEA concentration up to 0.55 loading. While in the concentrations of protonated MEA ($MEAH^+$) and MEA carbamate ($MEACOO^-$), a sudden increase is observed and in charge of 0.133, the $MEACOO^-$ ion reaches its maximum concentration of 0.3257. Also, the concentration of H^+ and OH^- ions can be neglected. Similar behavior was observed for other amine concentrations. According to the previous modeling results in the literature for MEA + CO_2+ H_2O system, a similar trend for component concentrations was observed (Wang et al., 2004 and Zhang et al., 2011). Figures 21, 22, and 23 show the component concentrations of MEA–CO_2–H_2O system in the liquid phase.

3.11. Gas phase mole fractions

Figures 24 and 25 show the mole fraction of CO_2 and H_2O in the gas phase, respectively. With increasing pressure, the mole fraction of water in the gas phase decreases, and the mole fraction of CO_2 has an upward trend.

3.12. Model validation

The modeling results in Figure 26 show that there is a good agreement between the experimental data and the estimated CO_2 loading. Relative and percentage error for the reported data is shown in Table 7. The minimum and maximum error rates for this system are 5.12 and 13.86 %, respectively. The errors can be due to a laboratory error and the omission of some existing interactions. Thus, the Pitzer model can predict the corresponding experimental data with a good approximation.

Table 9. CO_2 absorption capacity in the amine solutions in presence of solid sorbents.

Sample	Activated carbon type	Maximum uptake (mg/g)	The amount of solution and AC used	T (°C)	Ref
AC-MEA	Commercial activated carbon: Palm shell activated carbon	49.00	0.2, w/w, AMP, MEA/deionized water, 5 gr of AC	25	(Khalil et al., 2012)
Non-impregnated activated carbon		18.00		25	
AC-AMP	Commercial activated carbon: Palm shell activated carbon	34.00		25	
Non-impregnated activated carbon		18.00		25	
Native AC	Commercial activated carbon: Palm shell activated carbon	44.44	5 mL of 3% w/v MEA/DEA in methanol, 1 gr of AC	40	(Kongnoo et al., 2016)
		36.96		50	
		29.04		60	
		21.56		70	
AC-MEA	Commercial activated carbon: Palm shell activated carbon	44.80		40	
		51.92		50	
		58.52		60	
		65.12		70	
AC-DEA	Commercial activated carbon: Palm shell activated carbon	52.80		40	
		59.40		50	
		66.00		60	
		72.16		70	
AC-TEA	Commercial activated carbon: coke	22.26	5.5 wt% of TEA, 0.6 gr of AC	40	(Khoshraftar et al., 2021)
AC-MEA	Walnut-shell waste	30.23	5.5 wt% of MEA, 0.6 gr of AC	40	this work

3.13. Optimization

Optimum values of variables are determined using RSM to achieve the best CO_2 loading response. CO_2 uptake was selected to achieve maximum performance. Table 8 presents the optimization of CO_2 loading parameters using experimental design software.

3.14. Comparison of absorption loading with various solid sorbents

In this research, the absorption capacity of MEA solution in presence of activated carbon was compared with other amine solutions. The comparison results is shown in Table 9. The results show that different amounts of activated carbons was used in the previous works. The results of this study can be used to improve a new activated carbon via green synthesis as a solid adsorbent in the MEA solution that is effective for CO_2 absorption.

4. Conclusion

The advantages of using activated carbon particles in the amine solutions include increasing the surface of gas-liquid transfer, cheapness, and availability. In this research, CO_2 uptake in the presence and absence of activated carbon particles in MEA solution has been investigated. The experiments were performed at different operating conditions including temperature in range of 20–60 °C, pressure in range of 3.5–9.5 bar, MEA concentration in range of 2.5–8.5 wt% and activated carbon in range of 0–0.9 g/L. RSM has conducted a variety of tests to investigate the effects of operational parameters on the process response. The optimal values of independent variables to achieve the maximum absorption rate include temperature of 30 °C, pressure of 5.193 bar, MEA solution of 7 wt%, and activated carbon of 0.75 g/L. According to the results, addition of activated carbon from the waste walnut shell to MEA solution improves the absorption performance.

Declarations

Author contribution statement

Zohreh Khoshraftar & Ahad Ghaemi: Conceived and designed the experiments; Performed the experiments; Analyzed and interpreted the data; Contributed reagents, materials, analysis tools or data; Wrote the paper.

Funding statement

This research did not receive any specific grant from funding agencies in the public, commercial, or not-for-profit sectors.

Data availability statement

Data included in article/supp. material/referenced in article.

Declaration of interests statement

The authors declare no conflict of interest.

Additional information

Supplementary content related to this article has been published online at https://doi.org/10.1016/j.heliyon.2021.e08689.

References

Amiri, M., Shahhosseini, S., Ghaemi, A., 2017. Optimization of CO_2 capture process from simulated flue gas by dry regenerable alkali metal carbonate based adsorbent using response surface methodology. Energy Fuel. 31, 5286–5296.

Aschenbrenner, O., Styring, P., 2010. Comparative study of solvent properties for carbon dioxide absorption. Energy Environ. Sci. 3, 1106–1113.

Behroozi, A.H., Akbarzad, N., Ghaemi, A., 2020. CO_2 reactive absorption into an aqueous blended MDEA and TMS solution: experimental and modeling. Int. J. Environ. Res. 14, 347–363.

Behroozi, A.H., Saeidi, M., Ghaemi, A., Hemmati, A., Akbarzad, N., 2021. Electrolyte solution of MDEA–PZ–TMS for CO_2 absorption; response surface methodology and equilibrium modeling. Environ. Technol. Innovat. 23, 101619.

Beri, K.Y.V., Barbosa, D.P., Zbair, M., Ojala, S., de Oliveira, S.B., 2021. Adsorption of Estradiol from aqueous solution by hydrothermally carbonized and steam activated palm kernel shells. Energy Nexus 100009.

Bougie, F., Iliuta, M.C., 2011. CO_2 absorption in aqueous piperazine solutions: experimental study and modeling. J. Chem. Eng. Data 56, 1547–1554.

Donaldson, T.L., Nguyen, Y.N., 1980. Carbon dioxide reaction kinetics and transport in aqueous amine membranes. Ind. Eng. Chem. Fundam. 19, 260–266.

Gabrielsen, J., Michelsen, M.L., Stenby, E.H., Kontogeorgis, G.M., 2005. A model for estimating CO_2 solubility in aqueous alkanolamines. Ind. Eng. Chem. Res. 44, 3348–3354.

Gao, P., Zhou, Y., Meng, F., Zhang, Y., Liu, Z., Zhang, W., Xue, G., 2016. Preparation and characterization of hydrochar from waste eucalyptus bark by hydrothermal carbonization. Energy 97, 238–245.

Ghaemi, A., Mashhadimoslem, H., Zohourian Izadpanah, P., 2021. NiO and MgO/activated carbon as an efficient CO_2 adsorbent: characterization, modeling, and optimization. Int. J. Environ. Sci. Technol. 1–20.

Gholamiyan, S., Hamzehloo, M., Farrokhnia, A., 2020. RSM optimized adsorptive removal of erythromycin using magnetic activated carbon: adsorption isotherm, kinetic modeling and thermodynamic studies. Sustain. Chem. Pharm. 17, 100309.

González, B., Manyà, J.J., 2020. Activated olive mill waste-based hydrochars as selective adsorbents for CO_2 capture under postcombustion conditions. Chem. Eng. Process. Intensif. 149, 107830.

Gupta, M., Coyle, I., Thambimuthu, K., 2003. CO_2 capture technologies and opportunities in Canada. In: 1st Canadian CC\\&S Technology Roadmap Workshop, p. 19.

Jane, I.-S., Li, M.-H., 1997. Solubilities of mixtures of carbon dioxide and hydrogen sulfide in water+ diethanolamine+ 2-amino-2-methyl-1-propanol. J. Chem. Eng. Data 42, 98–105.

Karami, B., Ghaemi, A., 2021. Cost-effective nanoporous hypercross-linked polymers could drastically promote the CO_2 absorption rate in amine-based solvents, improving energy-efficient CO_2 capture. Ind. Eng. Chem. Res.

Karbalaei Mohammad, N., Ghaemi, A., Tahvildari, K., Sharif, A.A.M., 2020. Experimental investigation and modeling of CO_2 adsorption using modified activated carbon. Iran. J. Chem. Chem. Eng. 39, 177–192.

Karnwiboon, K., Saiwan, C., Idem, R., Supap, T., Tontiwachwuthikul, P., 2017. Solvent extraction of degradation products in amine absorption solution for CO_2 capture in flue gases from coal combustion: effect of amines. Energy Proc. 114, 1980–1985.

Khajeh, M., Ghaemi, A., 2021. Strontium hydroxide-modified nanoclay montmorillonite for CO_2 capture: response surface methodology and adsorption mechanism. Int. J. Environ. Anal. Chem. 1–26.

Khajeh, M., Ghaemi, A., 2020. Exploiting response surface methodology for experimental modeling and optimization of CO_2 adsorption onto NaOH-modified nanoclay montmorillonite. J. Environ. Chem. Eng. 8, 103663.

Khalil, S.H., Aroua, M.K., Daud, W.M.A.W., 2012. Study on the improvement of the capacity of amine-impregnated commercial activated carbon beds for CO_2 adsorbing. Chem. Eng. J. 183, 15–20.

Khodadadi, M.J., Riahi, S., Abbasi, M., 2019. Experimental modeling of the solubility of carbon dioxide in aqueous solution of monoethanolamine+ 1, 3-diaminopropane. J. Mol. Liq. 281, 415–422.

Khoshraftar, Z., Ghaemi, A., Sigaroodi, A.H.M., 2021. The effect of solid adsorbents in Triethanolamine (TEA) solution for enhanced CO_2 absorption rate. Res. Chem. Intermed. 1–20.

Khoshraftar, Z., Shamel, A., 2016. Adsorption of Malachite green dye from aqueous solutions using roots of Azolla filiculoides. J. Phys. Theor. Chem. 13, 237–252.

Kongnoo, A., Intharapat, P., Worathanakul, P., Phalakornkule, C., 2016. Diethanolamine impregnated palm shell activated carbon for CO_2 adsorption at elevated temperatures. J. Environ. Chem. Eng. 4, 73–81.

Leonzio, G., 2017. Optimization through response surface methodology of a reactor producing methanol by the hydrogenation of carbon dioxide. Processes 5, 62.

Leung, D.Y.C., Caramanna, G., Maroto-Valer, M.M., 2014. An overview of current status of carbon dioxide capture and storage technologies. Renew. Sustain. Energy Rev. 39, 426–443.

Littel, R.J., Van Swaaij, W.P.M., Versteeg, G.F., 1990. Kinetics of carbon dioxide with tertiary amines in aqueous solution. AIChE J. 36, 1633–1640.

Lv, B., Guo, B., Zhou, Z., Jing, G., 2015. Mechanisms of CO_2 capture into monoethanolamine solution with different CO_2 loading during the absorption/desorption processes. Environ. Sci. Technol. 49, 10728–10735.

Ma'mun, S., Nilsen, R., Svendsen, H.F., Juliussen, O., 2005. Solubility of carbon dioxide in 30 mass % monoethanolamine and 50 mass\\% methyldiethanolamine solutions. J. Chem. Eng. Data 50, 630–634.

Mannel, D.S., Qi, G., Widger, L.R., Bryant, J., Liu, Kun, Fegenbush, A., Lippert, C.A., Liu, Kunlei, 2017. Enhancements in mass transfer for carbon capture solvents part II: micron-sized solid particles. Int. J. Greenh. Gas Contr. 61, 138–145.

Mirzaei, F., Ghaemi, A., 2020. Mass transfer modeling of CO_2 absorption into blended aqueous MDEA–PZ solution. Iran. J. Oil Gas Sci. Technol. 9, 77–101.

Monastersky, R., 2013. Global carbon dioxide levels near worrisome milestone. Nat. News 497, 13.

Naeem, S., Ghaemi, A., Shahhosseini, S., 2016. Experimental investigation of CO_2 capture using sodium hydroxide particles in a fluidized bed. Kor. J. Chem. Eng. 33, 1278–1285.

Park, J.-Y., Yoon, S.J., Lee, H., Yoon, J.-H., Shim, J.-G., Lee, J.K., Min, B.-Y., Eum, H.-M., Kang, M.C., 2002a. Solubility of carbon dioxide in aqueous solutions of 2-amino-2-ethyl-1, 3-propanediol. Fluid Phase Equil. 202, 359–366.

Najafi, P., Penchah, H.R., Ghaemi, A., 2021. Synthesis and characterization of Benzyl chloride-based hypercrosslinked polymers and its amine-modification as an adsorbent for CO_2 capture. Environ. Technol. Innov. 23, 101746.

Park, S.H., Lee, K.B., Hyun, J.C., Kim, S.H., 2002b. Correlation and prediction of the solubility of carbon dioxide in aqueous alkanolamine and mixed alkanolamine solutions. Ind. Eng. Chem. Res. 41, 1658–1665.

Pashaei, H., Ghaemi, A., Nasiri, M., 2017. Experimental investigation of CO_2 removal using Piperazine solution in a stirrer bubble column. Int. J. Greenh. Gas Contr. 63, 226–240.

Pashaei, H., Ghaemi, A., Nasiri, M., Karami, B., 2020. Experimental modeling and optimization of CO_2 absorption into piperazine solutions using RSM-CCD methodology. ACS Omega 5, 8432–8448.

Penchah, H.R., Ghaemi, A., Godarziani, H., 2021. Eco-friendly CO_2 adsorbent by impregnation of diethanolamine in nanoclay montmorillonite. Environ. Sci. Pollut. Res. 1–17.

Ramezani, R., Bernhardsen, I.M., Di Felice, R., Knuutila, H.K., 2021. Physical properties and reaction kinetics of CO_2 absorption into unloaded and CO2 loaded viscous monoethanolamine (MEA) solution. J. Mol. Liq. 329, 115569.

Ramezanipour Penchah, H., Ghaemi, A., Jafari, F., 2021. Piperazine-modified activated carbon as a novel adsorbent for CO_2 capture: modeling and characterization. Environ. Sci. Pollut. Res. 1–10.

Ran, H., Wang, J., Abdeltawab, A.A., Chen, X., Yu, G., Yu, Y., 2017. Synthesis of polymeric ionic liquids material and application in CO_2 adsorption. J. Energy Chem. 26, 909–918.

Rashidi, N.A., Yusup, S., 2017. Potential of palm kernel shell as activated carbon precursors through single stage activation technique for carbon dioxide adsorption. J. Clean. Prod. 168, 474–486.

Rinprasertmeechai, S., Chavadej, S., Rangsunvigit, P., Kulprathipanja, S., 2012. Carbon dioxide removal from flue gas using amine-based hybrid solvent absorption. Int. J. Chem. Biomol. Eng. 6, 296–300.

Saeidi, M., Ghaemi, A., Tahvildari, K., Derakhshi, P., 2018. Exploiting response surface methodology (RSM) as a novel approach for the optimization of carbon dioxide adsorption by dry sodium hydroxide. J. Chin. Chem. Soc. 65, 1465–1475.

Shahbazi, A., Nasab, B.R., 2016. Carbon capture and storage (CCS) and its impacts on climate change and global warming. J. Petrol Environ. Biotechnol. 7.

Shao, L., Sang, Y., Huang, J., 2019. Imidazole-based hyper-cross-linked polymers derived porous carbons for CO_2 capture. Microporous Mesoporous Mater. 275, 131–138.

Shen, K.P., Li, M.H., 1992. Solubility of carbon dioxide in aqueous mixtures of monoethanolamine with methyldiethanolamine. J. Chem. Eng. Data 37, 96–100.

Songolzadeh, M., Soleimani, M., Takht Ravanchi, M., Songolzadeh, R., 2014. Carbon dioxide separation from flue gases: a technological review emphasizing reduction in greenhouse gas emissions. Sci. World J. 2014.

Tong, C., Perez, C.C., Chen, J., Marcos, J.-C.V., Neveux, T., Le Moullec, Y., 2013. Measurement and calculation for CO_2 solubility and kinetic rate in aqueous solutions of two tertiary amines. Energy Proc. 37, 2084–2093.

Wagner, M., von Harbou, I., Kim, J., Ermatchkova, I., Maurer, G., Hasse, H., 2013. Solubility of carbon dioxide in aqueous solutions of monoethanolamine in the low and high gas loading regions. J. Chem. Eng. Data 58, 883–895.

Wang, L., Li, Y., Li, S., Ji, P., Jiang, C., 2014. Preparation of composite poly (ether block amide) membrane for CO_2 capture. J. Energy Chem. 23, 717–725.

Wang, R., Li, D.F., Liang, D.T., 2004. Modeling of CO_2 capture by three typical amine solutions in hollow fiber membrane contactors. Chem. Eng. Process. Process Intensif. 43, 849–856.

Wang, W., Zhou, M., Yuan, D., 2017. Carbon dioxide capture in amorphous porous organic polymers. J. Mater. Chem. A 5, 1334–1347.

Wu, Y., Xu, J., Mumford, K., Stevens, G.W., Fei, W., Wang, Y., 2020. Recent advances in carbon dioxide capture and utilization with amines and ionic liquids. Green Chem. Eng.

Yang, M., Guo, L., Hu, G., Hu, X., Chen, J., Shen, S., Dai, W., Fan, M., 2016. Adsorption of CO_2 by petroleum coke nitrogen-doped porous carbons synthesized by combining ammoxidation with KOH activation. Ind. Eng. Chem. Res. 55, 757–765.

Zheng, Y., Guo, D., Dong, L., Chen, J., 2011. Simulation and pilot plant measurement for CO_2 absorption with mixed amines. Energy Proc. 4, 299–306.